Failure analysis of thin metal foils

G. Bolzon, M. Shahmardani
Politecnico di Milano, Department of civil and environmental engineering, Italy
Gabriella.bolzon@polimi.it, Mahdieh.shahmardani@polimi.it

R. Liu, E. Zappa
Politecnico di Milano, Department of mechanical engineering, Italy
Rui.liu@polimi.it, Emanuele.zappa@polimi.it

ABSTRACT. The mechanical response and the failure mode of thin metal foils under tensile load has been analyzed supplementing the usual test records with full-field measurements performed by three-dimensional digital image correlation (3D DIC) techniques. The experiments have been simulated by finite element models formulated within a non-linear continuum framework. The study presented in this contribution concerns symmetrically pre-cracked aluminum samples. The wrinkling of the specimens during the test and the possible and alternative failure mechanisms are evidenced and discussed.

KEYWORDS. Thin metal foils; Failure analysis; Digital image correlation; Numerical simulation.

Citation: Bolzon, G., Shahmardani, M., Liu, R., Zappa, E., Failure analysis of thin metal foils, Frattura ed Integrità Strutturale, 42 (2017) 328-336.

Received: 08.08.2017
Accepted: 24.08.2017
Published: 01.10.2017

INTRODUCTION

The present study is motivated by the spreading application of thin metal foils in different technological fields, for the production of flexible electronics, nano or micro-devices and beverages packaging [1-3]. The thinness of these laminates (few microns or less) makes them behave differently from the corresponding bulk materials. In particular, the apparent brittleness increases as the metal thickness is reduced [4-6].
Determining the actual material properties and fracture characteristics of thin foils may be rather problematic since the samples are difficult to handle and sensitive to local imperfections, size and geometric effects. In these conditions, even the interpretation of the output of uniaxial tensile tests may be difficult [7, 8].
Alternative loading procedures [9] and full-field displacement monitoring combined with the simulation of the experiment [10, 11] have been suggested to overcome some limitations of the most commonly employed parameter calibration procedures. Different numerical approaches have been proposed in the present context [12, 13].
This study focuses on the mechanical response of thin aluminum (Al) samples leaded to failure under uniaxial tensile load. Symmetrically cut edge notches induce crack propagation in a pre-fixed location. The displacement distribution and the

configuration changes of the specimens are monitored by a three-dimensional digital image correlation (3D DIC) system [14]. The tests are simulated by two and three-dimensional numerical models of the experiment.

EXPERIMENTAL SETUP

In the present investigation, thin Al foils (9 μm nominal thickness) are subjected to quasi-static uniaxial loading under displacement control. The testing system (MTS Synergie 200) is shown in Fig. 1(a). The material samples fixed on the machine clamps have dimensions comparable with those considered in former investigations [15], namely 250 mm length and 100 mm width. Two notches 10 mm long are symmetrically cut at both specimen sides as sketched in Fig. 1(b).

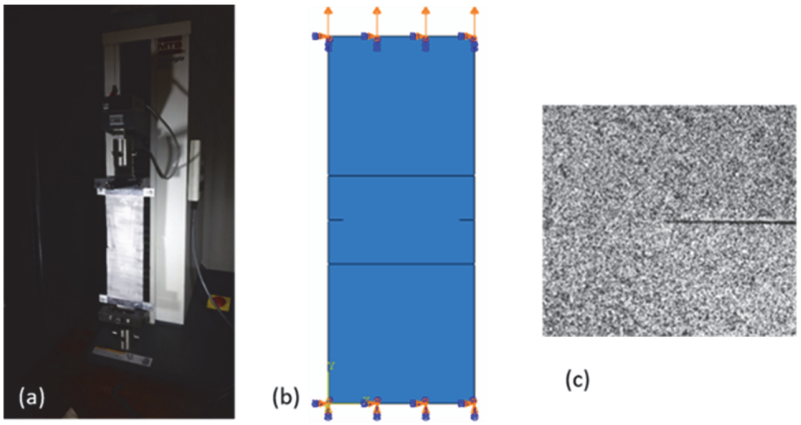

Figure 1: Experimental setup (a), schematized testing conditions (b) and speckle pattern (c).

The images to be processed by 3D DIC technique are acquired during the test. The stereoscopic cameras point to the specimen that is properly illuminated by two LED-based lighting devices. The exposure time of the cameras, the light intensity and the projection angle with respect to the specimen are optimized in order to avoid image saturation and reduce the specular reflection due to out-of-plane displacements. The image acquisition and the synchronization of the two cameras is controlled by means of an external trigger. The image acquisition frequency is set to 1 Hz in order to follow the fracture propagation under the loading rate of 1 mm/min.

A high resolution vision system is required to detect the whole spatial deformation of the samples and to accurately track the propagation of the two cracks emerging from the initial notches. These requirements are satisfied by a pair of GX3300 cameras with full resolution 3296×2472 pixel (px), equipped with 50 mm focal length optics (Zeiss Makro Planar T 2/50). The obtained image resolution is about 15 px/mm.

The accuracy of DIC analysis is strongly related to the texture of the monitored objects and to the pre-processing of the images, see [16]. Correlation results are therefore improved by random speckles generated on the surface of the specimen with high contrast with respect to the background [17]. To prevent specular reflection, the metal surface is painted white before creating black dots using an airbrush. The nozzle size and the air pressure are tuned in order to produce the optimal speckle size (around 4-5 pixels on average). Fig. 1(c) displays the pattern obtained in the vicinity of the crack tip in one of the tested samples.

EXPERIMENTAL RESULTS

The sequence of snapshots reported in Fig. 2 visualizes the cracks emerging from the initial notches cut in the metal sample as the displacement of the head of the testing machine increases. The left side of the images corresponds to the fixed clamp at the bottom of the tension instrument shown in Fig. 1, while the moving clamp (at the top in the machine) is on the right.

Fig. 3 shows the local distribution of the material elongation in the loading direction at 1 mm overall displacement. These measurements are obtained by 3D DIC processing. Strain concentration permits to locate accurately the position of the crack tip. Notice that the graph in Fig. 3 suggests the existence of large values also along the fractured edges. These meaningless values are a consequence of the strain computation algorithm that does not account for the displacement

discontinuity generated by the crack opening. The visual superposition of the digital image and of the reconstructed field avoids any misinterpretation of the results.
A characteristic feature of the tests performed on thin metal foils is the appearance of wrinkles ahead of the fracture zone, see the bright strips in Fig. 2. 3D DIC permits to reconstruct the out-of-plane displacement distribution, represented in Fig. 4 in correspondence of four different loading steps. The fractured edges undergo the largest deflection from planarity but the foil corrugates in the ligament region as well, as shown by the measurements reported in Fig. 5. Notice that the mean out-of-plane displacement is almost null all along the test, while the maximum values increase significantly in the softening regime, i.e. starting from about 1 mm relative displacement, see Fig. 5(a) and Fig. 6(a). On the contrary, the depth of the wrinkles developing in the ligament increases almost monotonically with the load up to the peak of the reaction force, and then reduces.
The almost symmetric fracture propagation during the test is confirmed by the graphs in Fig. 6(b), visualizing the crack growth as the overall displacement increases. The crack length is evaluated as the distance between the current and the initial position of the relevant tip.

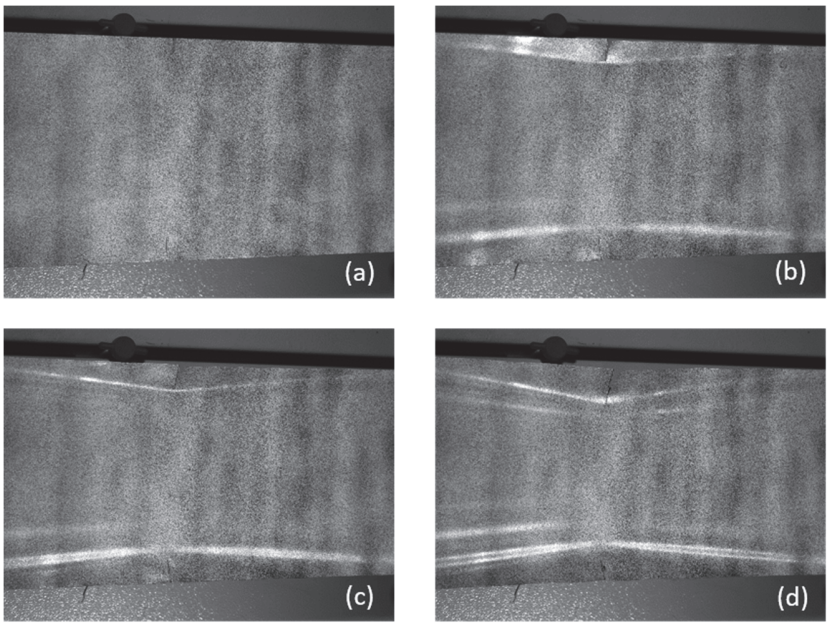

Figure 2: Snapshot sequence during the test, in the initial configuration (a) and at overall displacement 0.5 mm (b), 0.75 mm (c) and 1 mm (d).

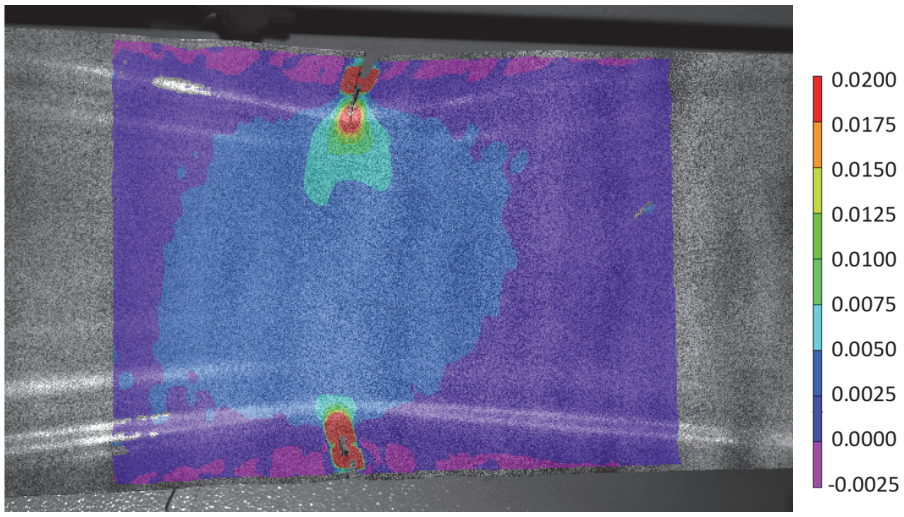

Figure 3: Strain component along the loading direction at 1 mm overall displacement.

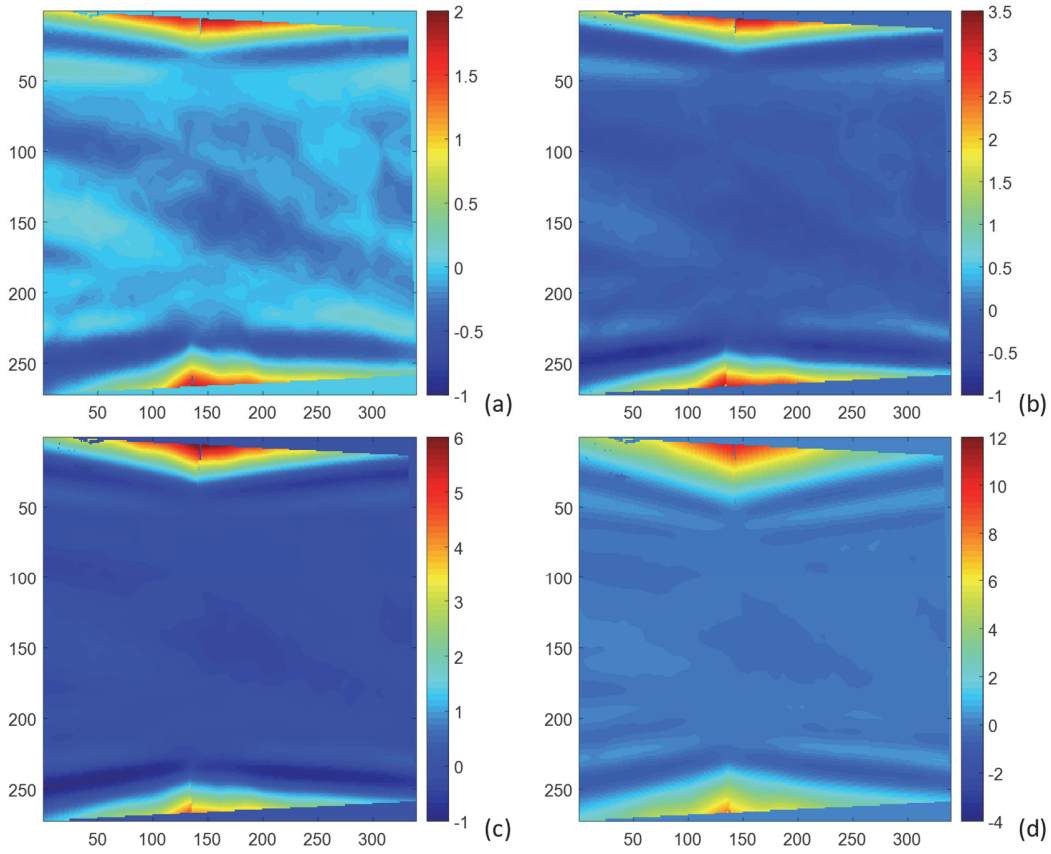

Figure 4: Out-of-plane displacement distribution (mm scale) corresponding to the overall displacement 0.25 mm (a), 0.5 mm (b), 0.75 mm (c) and 1 mm (d).

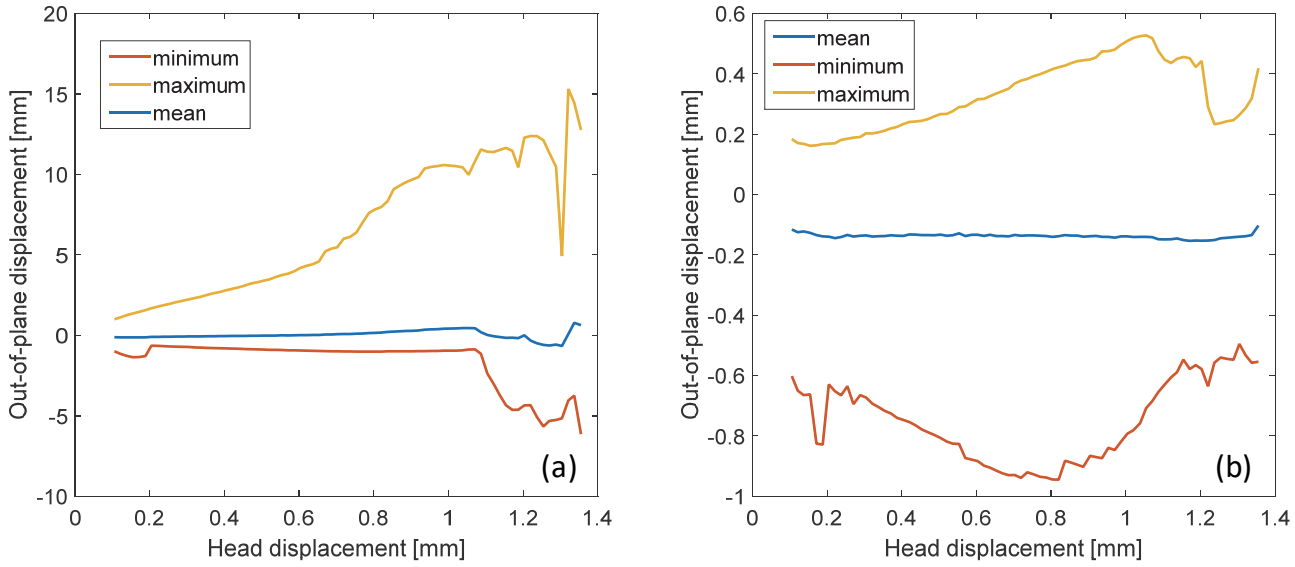

Figure 5: Out-of-plane displacements in the monitored area (a) and in the ligament region (b).

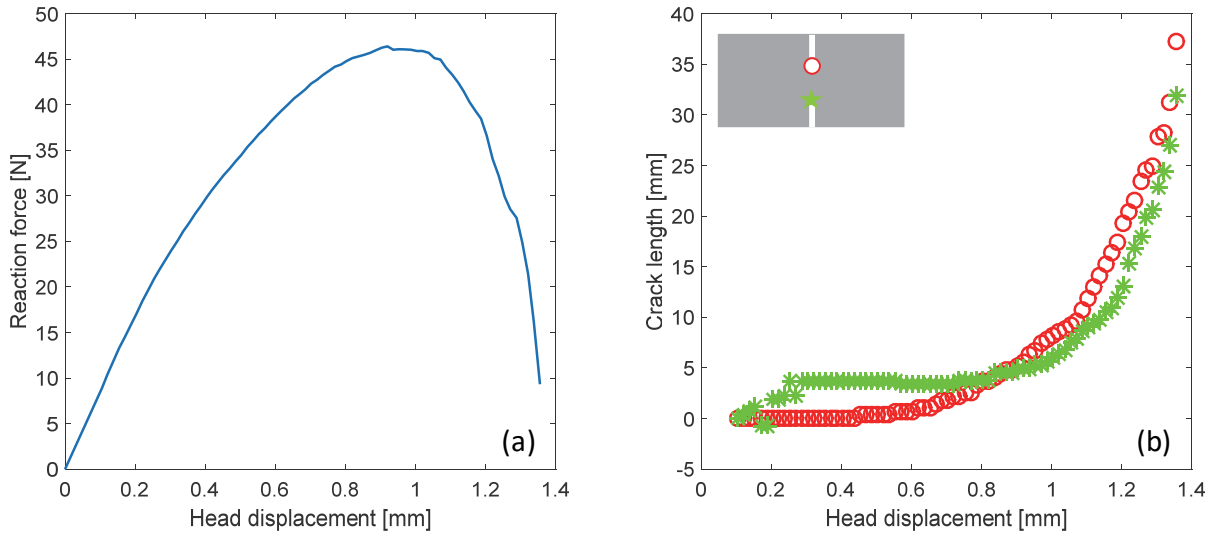

Figure 6: Reaction force (a) and crack propagation (b) during the test.

NUMERICAL ANALYSIS

The performed experiments are simulated by the finite element method, using a commercial code that implements both material and geometrical non-linearity [18]. Either two-dimensional (2D) and three-dimensional (3D) quasi-static analyses are carried out, introducing a small damping coefficient as numerical stabilizing factor to improve convergence. The boundary conditions that reproduce the clamped supports in the plane of the Al foil are schematized in Fig. 1. The problem domain is discretized by the regular and random fine meshes visualized in Fig. 8, made of 4-node elements representing either plane stress, or membrane, or shell conditions.
Large plastic deformation with small elastic strains are assumed. An additive decomposition of the total strains into the elastic and plastic components is thus introduced. The considered Al samples exhibit a slight anisotropy, which is neglected in the simulations. The metal response is therefore described by the classical elastic-plastic constitutive law based on Hencky-Huber-von Mises yield criterion with isotropic hardening and associative flow rule.

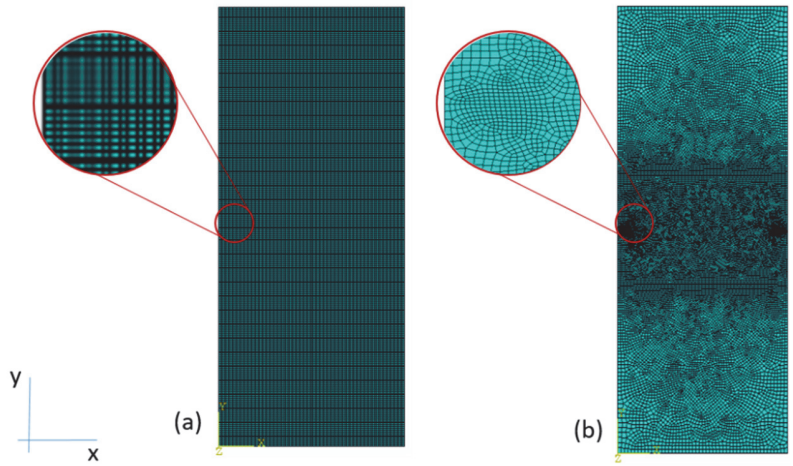

Figure 7: Regular (a) and random (b) discretization of the edge-notched Al-foil and the assumed reference system.

The initial elastic relationship between the true (Cauchy) stress components and the corresponding logarithmic strains is assumed to be linear, characterized by the elastic modulus E and by the lateral contraction ratio ν.
The elastic domain is defined in terms of the stress components acting in the plane x-y (Fig. 7) as follows:

$$f = \sigma_{xx}^2 + \sigma_{yy}^2 - \sigma_{xx}\sigma_{yy} + 3\sigma_{xy}^2 \le \bar{\sigma}^2 \tag{1}$$

The limit $\bar{\sigma}$ initially evolves according to the relationship:

$$\bar{\sigma} = \bar{\sigma}_0 \left(1 + \frac{E\bar{\varepsilon}^p}{\bar{\sigma}_0} \right)^n \tag{2}$$

where $\bar{\sigma}_0$ and n are material parameters (initial yield limit and hardening exponent) while $\bar{\varepsilon}^p$ represents the equivalent plastic strain:

$$\bar{\varepsilon}^p = \sqrt{\frac{2}{3}\left(\varepsilon_{xx}^p\right)^2 + \frac{2}{3}\left(\varepsilon_{yy}^p\right)^2 + \frac{1}{3}\left(\varepsilon_{xy}^p\right)^2} \tag{3}$$

Each plastic strain component entering in relation (3) is defined in rates by the associative flow rule; for instance:

$$\dot{\varepsilon}_{xx}^p = \dot{\lambda}\frac{\partial f}{\partial \sigma_{xx}} \quad \text{(and similar ones)} \tag{4}$$

The variable λ introduced with relation (4) represents the plastic multiplier.

The function $\bar{\sigma}\left(\bar{\varepsilon}^p\right)$ is assumed constant beyond the threshold value that defines the material tensile strength $\bar{\sigma}_u$.

The constitutive parameters used in the present analyses are listed in Tab. 1. They return the envelope of the uniaxial stress-strain curves obtained from plain material samples [7], and are consistent with those employed in former studies [3, 8, 15].

Young's modulus E [GPa]	Poisson ratio ν [-]	Yield limit $\bar{\sigma}_0$ [MPa]	Tensile strength $\bar{\sigma}_u$ [MPa]	Hardening exponent n [-]
46	0.3	35	72.5	0.015

Table 1: Material properties.

The response of the Al foil is represented in Fig. 8 in terms of the engineering (nominal) stress and strain values. The computational results obtained by either plane stress (2D) conditions and 3D membrane and shell simulations are compared with the experimental output (dots). The considered measurements consist of the reaction force recorded by the loading machine and of the relative displacements of the end points of segments AB, CD and EF represented in the insert of the figure. These local variables are recovered by 3D DIC and concern the three specimens named sp7, sp8 and sp9. The relevant plots are rather repetitive, confirming that the cracks emanating from the two notches progress regularly and in an almost symmetric manner.

The experimental and the numerical output matches well in the initial phase of the test, but the overall strength is not captured by any of the performed simulations. The results of the numerical analyses differ as the maximum load is approached and beyond, although the in-plane formulation of the considered finite element types is almost the same.

The simulated deformation and failure modes are suggested by the graphs drawn in Fig. 9, which refer to 3.75 mm overall displacement (i.e., 1.5% nominal strain) in the case of random meshes. Regular discretization does not introduce substantial modifications. It is worth noticing that membrane elements return strain localization where fracture eventually occurs. The consequent thickness reduction in the ligament is reflected by the significant decay of the nominal stress in the post-peak (softening) regime. On the contrary, 2D plane stress and 3D shell models suggest shear band failure mode.

The appearance of wrinkles ahead of the notch tips is reproduced only by the 3D simulation performed by shell elements, which returns the maximum load reduced as shown in Fig. 8(a).

The local distributions drawn in Fig. 10 and Fig. 11 evidence compression stresses acting in the direction orthogonal to the applied external load. These components are likely responsible of the instability phenomenon leading to the wrinkle formation.

The graphs in Fig. 8(b) confirm that wrinkles appear in the early stage of the experiment. Fig. 9 to Fig. 11 show a large number of wrinkles with narrow spacing away from the ligament area. However, the amplitudes obtained from the computations are smaller than those observed in reality.

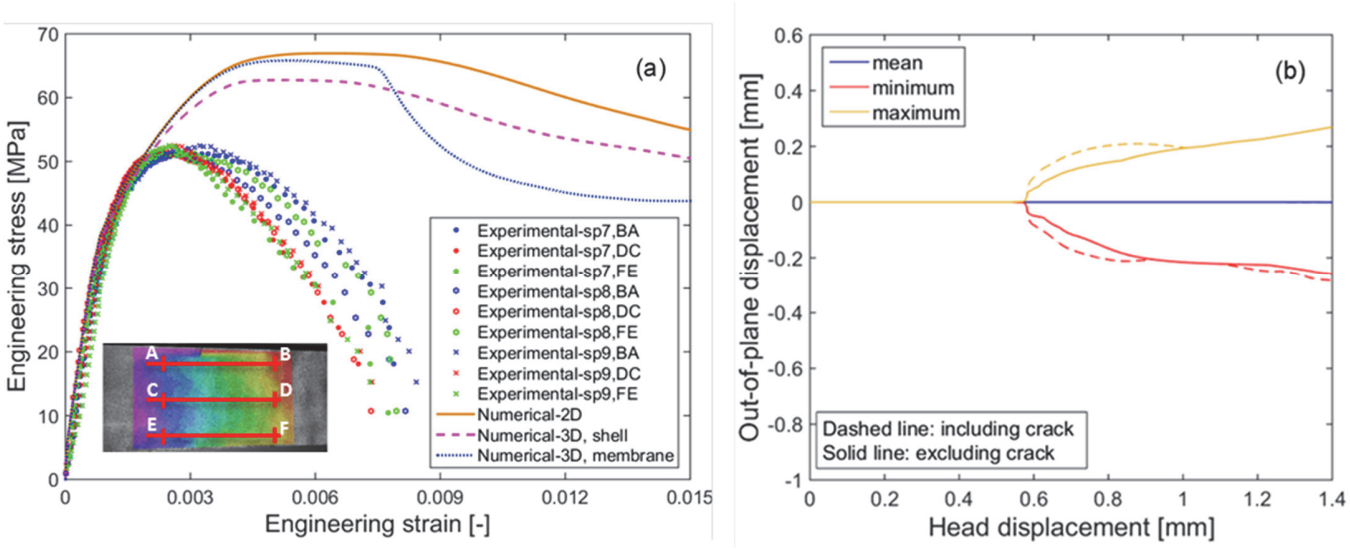

Figure 8: Simulated material response compared with the experimental output (a) and the out-of-plane displacements recovered from shell model (b).

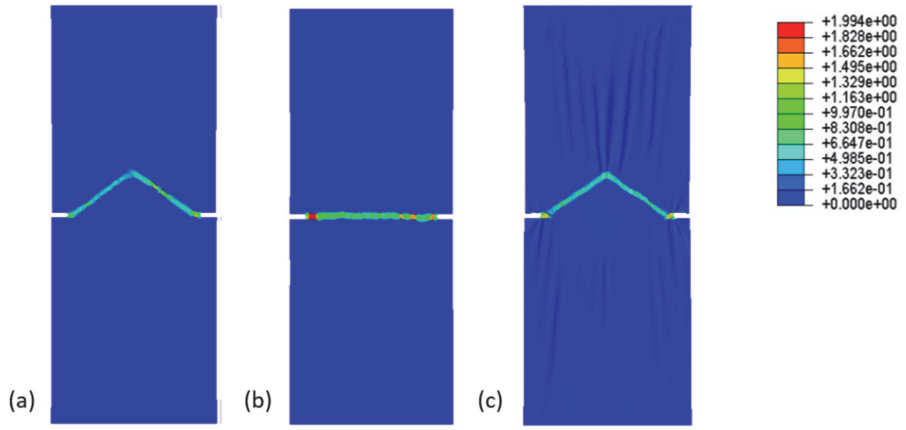

Figure 9: Plastic strain distribution for 1.5% nominal strain in plane stress (a), membrane (b) and shell (c) analyses.

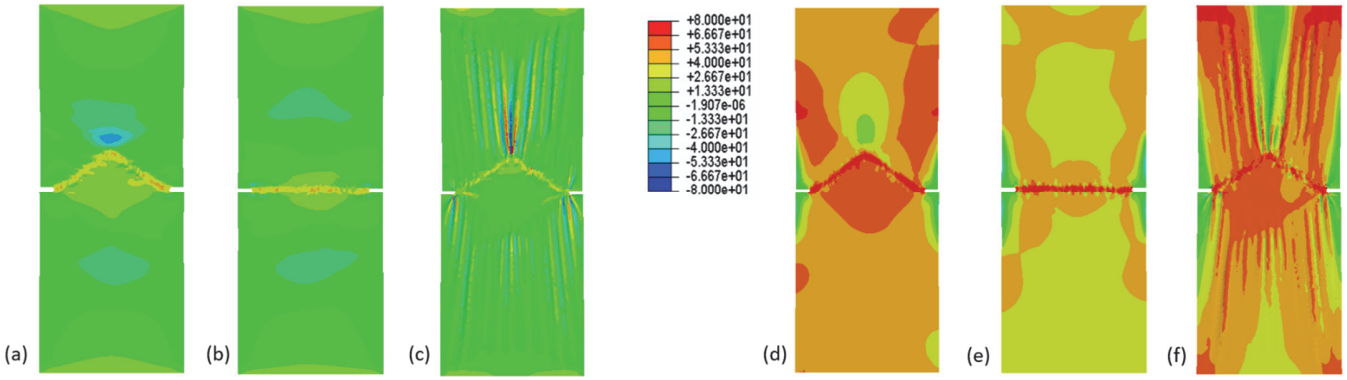

Figure 10: Local stress distribution for 1.5% nominal strain along direction x (a, b, c) and y (d, e, f) obtained from plane stress (a, d), membrane (b, e) and shell (c, f) analyses.

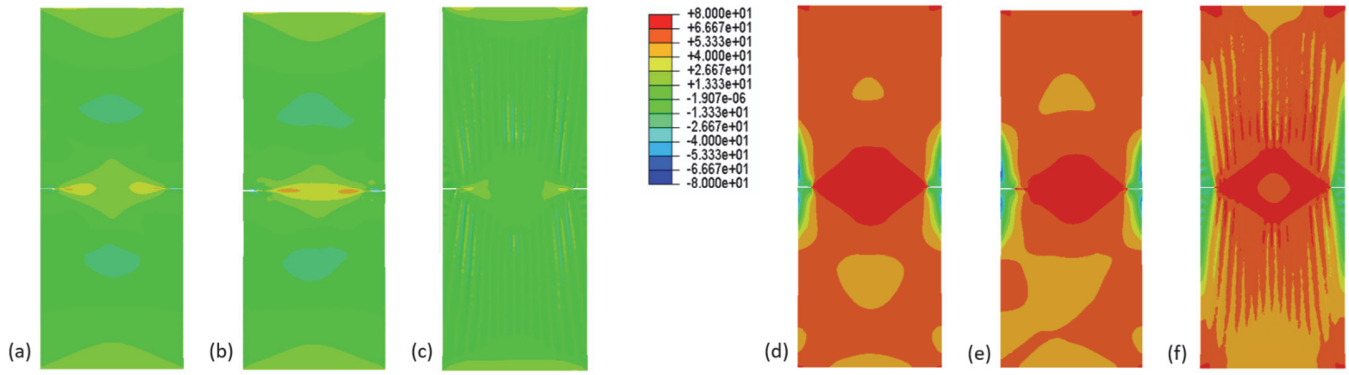

Figure 11: Local stress distribution at the maximum load along direction x (a, b, c) and y (d, e, f) obtained from plane stress (a, d), membrane (b, e) and shell (c, f) analyses.

CLOSING REMARKS

The mechanical response of thin aluminum (Al) samples under uniaxial tensile load has been investigated by experimental and numerical approaches. The displacement distribution and the configuration changes of the notched specimens have been monitored by a three-dimensional digital image correlation (3D DIC) system. The tests have been simulated in a finite element continuum context, taking into account both material and geometrical nonlinearities in quasi-static analyses.

The main phenomena observed in the real experiments have been reproduced to some extent by the computations but a complete agreement and quantitative assessment is still missing. The interaction between material and geometric instability, which makes the problem sensitive to several physical and modelling details, may be one reason of the discrepancies. Dynamics and material separation, not taken into account in the present work, are also expected to influence the simulation results. Further studies will be carried out in the next future.

REFERENCES

[1] Read, D.T., Volinski, A.A., Thin films for microelectronics and photonics: Physics, mechanics, characterization, and reliability. Ch. 4 in: Micro- and Opto-Electronic Materials and Structures: Physics, Mechanics, Characterization, Reliability, Packaging (Suhir, E.L., Lee, Y.C., Wong, C.P., Eds), Springer, New York, (2007) 135-180.

[2] Wong, W.S., Salleo, A. (Eds.), Flexible Electronics (Materials and Applications), Springer, New York, (2009).

[3] Bolzon G., Cornaggia G., Shahmardani M., Giampieri A., Mameli A., Aluminum laminates in beverage packaging: Models and experiences. Beverages, 1 (2015) 183–193.

[4] Klein, M., Hardboletz, A., Weiss, B., Khatibi, G., The 'size effect' on the stress–strain, fatigue and fracture properties of thin metallic foils, Materials Science and Engineering A, 319 (2001) 924–928.

[5] Hu, W., Characterised behaviours and corresponding yield criterion of anisotropic sheet metals, Materials Science and Engineering A, 345 (2003) 139–144.

[6] Wang, H.W., Kang, Y.L., Zhang, Z.F., Qin, Q.H, Size effect on the fracture toughness of metallic foil, International Journal of Fracture, 123 (2003) 177–185.

[7] Bolzon, G., Shahmardani, M., Liu, R., Zappa, E., A combined experimental-numerical investigation of the failure mode of thin metal foils, Procedia Structural Integrity, 3 (2017) 168–171.

[8] Kao-Walter, S., On the Fracture of Thin Laminates. Dissertation Series No. 2004:07, Blekinge Institute of Technology, Karlskrona, Sweden (2004).

[9] Li, C.H., Duan, Q.Q., Zhang, Z.F., Assessment of tearing resistance of ductile metals: Using a new concept of tearing toughness, Materials Science and Engineering A, 528 (2011) 1636-1640.

[10] Avril, S., Bonnet, M., Bretelle, A.S., Grediac, M., Hild, F., Ienny, P., Latourte, F., Lemosse, D., Pagano, S., Pagnacco, E., Overview of identification methods of mechanical parameters based on full-filed measurements, Experimental Mechanics, 48 (2008) 381-402.

[11] Bolzon, G., Advances in experimental mechanics by the synergetic combination of full-field measurement techniques and computational Tools, Measurement 54 (2014) 159–165.
[12] Roy, Y.A., and Dodds, R.H., Simulation of ductile crack growth in thin aluminum panels using 3-D surface cohesive elements, International Journal of Fracture 110 (2001) 21–45.
[13] Nielsen, K.L., Hutchinson J.W., Cohesive traction-separation laws for tearing of ductile metal plates, International Journal of Impact Engineering, 48 (2012) 15-23.
[14] Mathieu, F., Hild, F., Roux, S., Identification of a crack propagation law by digital image correlation, Journal of Fatigue, 36 (2012) 146-154.
[15] Andreasson, E., Kao-Walter, S., Ståhle, P., Micro-mechanisms of a laminated packaging material during fracture, Engineering Fracture Mechanics, 127 (2014) 313–326.
[16] Mazzoleni, P., Matta, F., Zappa, E., Sutton, M.A., Cigada, A., Gaussian pre-filtering for uncertainty minimization in digital image correlation using numerically-designed speckle patterns, Optics and Lasers in Engineering, 66 (2015) 19–33.
[17] Mazzoleni, P., Zappa, E., Matta, F., Sutton, Michael A. Thermo-mechanical toner transfer for high-quality digital image correlation speckle patterns, Optics and Lasers in Engineering, 75 (2015) 72–80
[18] Abaqus 6.10, 2015. Dassault Systèmes Simulia Corp.